Biology of Reproduction, 2018, 99(3), 536–545
doi:10.1093/biolre/ioy073
Research Article
Advance Access Publication Date: 24 March 2018

OXFORD

Research Article

Alteration of transporter activities in the epididymides of infertile initial segment-specific *Pten* knockout mice†

Bingfang Xu[1], Stephen D. Turner[2] and Barry T. Hinton[1,*]

[1]Department of Cell Biology, University of Virginia Health System, Charlottesville, Virginia, USA and [2]Bioinformatics Core, University of Virginia Health System, Charlottesville, Virginia, USA

*__Correspondence:__ Department of Cell Biology University of Virginia Health System PO Box 800732, Charlottesville, VA 22908, USA. Tel: 434-924-2174; Fax: 434-982-3912; E-mail: bth7c@virginia.edu

†__Grant support:__ This work was supported by the Eunice Kennedy Shriver NICHD/NIH grant HD068365.
Edited by Dr. Monika A. Ward, PhD, University of Hawaii John A. Burns School of Medicine

Received 1 January 2018; Revised 2 March 2018; Accepted 22 March 2018

Abstract

A fully functional initial segment, the most proximal region of the epididymis, is important for male fertility. Our previous study generated a mouse model to investigate the importance of initial segment function in male fertility. In that model, phosphatase and tensin homolog (*Pten*) was conditionally removed from the initial segment epithelium, which resulted in epithelial de-differentiation. When spermatozoa progressed through the de-differentiated epithelial duct, they developed angled flagella, suggesting compromised sperm maturation, which eventually resulted in male infertility. To understand the molecular mechanisms, by which PTEN regulates epididymal sperm maturation, we compared the transcriptome profile of the initial segment between controls and initial segment-specific *Pten* knockouts and revealed that water, ion, and organic solute transporter activities were one of the top molecular and cellular functions altered following loss of *Pten*. Alteration in protein levels and localization of several transporters following loss of *Pten* were also observed by immunofluorescence analysis. Epithelial cells of the initial segment from knockouts were more permeable to fluorescein isothiocyanate–dextran (4000 Da) compared to controls. Interestingly, conditional deletion of *Pten* from other organs also resulted in changes in transporter activity, suggesting a common role of PTEN in regulation of transporter activity. Taken together, our data support the hypothesis that loss of *Pten* from the initial segment epithelium results in changes in the transporting and permeability characteristics of the epithelium, which in turn altered the luminal fluid microenvironment that is so important for sperm maturation and male fertility.

Summary Sentence

Loss of *Pten* from the initial segment epithelium results in changes in the transporting and permeability characteristics of the epithelium, suggesting PTEN regulates epididymal water, ion, and organic solute transporter activities.

Key words: epididymis, PTEN, male infertility, transporter.

Introduction

Phosphatase and tensin homolog (PTEN) is a well-known tumor suppressor that is inactivated in a wide variety of human cancers [1]. In addition to its tumor suppressive function, PTEN has its role in embryogenesis and in the maintenance of normal physiological functions of many organ systems [1]. In our previous study, phosphatase and tensin homolog (*Pten*) was

conditionally deleted from the initial segment epithelium of the epididymis from postnatal day 17 onwards in mice, which did not result in cancer development in the epididymis but rather male infertility, suggesting that PTEN played a role in the maintenance of normal function of the epididymis [2].

Our previous study revealed that loss of *Pten* from the initial segment epithelium activated the AKT pathway, which suppressed the ERK pathway through inactivation of RAF1. The altered signal transduction pathways changed cell shape, size, and organization in the initial segment epithelium. These morphological changes reflected de-differentiation of the initial segment epithelium. When spermatozoa progressed through a de-differentiated epididymal duct, they developed angled flagella that prevented spermatozoa from reaching and fertilizing an egg in the female reproductive tract, which eventually resulted in male infertility [2].

Spermatozoa flagellar angulation was previously observed in other transgenically modified mouse models such as Ros1 proto-oncogene (*Ros1*) null mice [3] and transgenic mice carrying Simian virus 40 small T-antigen driven by glutathione peroxidase 5 (*Gpx5*) promoter [4]. Studies showed that flagellar angulation observed in these models was due to a dysfunction in volume regulation of spermatozoa [5–9]. Under normal physiological conditions, the epididymal lumen is rich in inorganic ions and small organic molecules which create an environment that is hyperosmotic relative to serum [10]. During normal epididymal transit, under a hyperosmotic lumen environment, spermatozoa acquire the capacity to regulate their cell volume. Thus, when spermatozoa are exposed to the iso-osmotic environment of the female tract, they are able to tolerate the sudden reduction in osmolality and their flagella remain straight [11]. In *Ros1* null mice, spermatozoa were not able to regulate volume, and when they encountered a lower osmolality in the female tract they developed flagellar angulation, which reduced spermatozoa motility and prevented fertilization [5–9]. Follow-up studies on *Ros1* null mice suggested that downregulation of glutamate transporter SLC1A1, also known as EAAC1, and alterations in luminal pH likely reflected the changes in epididymal luminal fluid environment, which affected normal sperm maturation [12, 13].

Although initial segment-specific *Pten* knockout mice, namely IS-specific *Pten* KOs, shared similar flagellar angulation phenotype with *Ros1* null mice, loss of *Pten* did not change *Ros1* mRNA levels. This suggested that PTEN did not signal though ROS1, thereby further suggesting that there was a different mechanism behind the similar flagellar angulation phenotype [2]. To investigate the mechanism(s) that resulted in the disruption of sperm maturation process in IS-specific *Pten* KOs, we employed RNAseq analysis to compare the transcriptome profiles of the initial segment of control and knockout mice. Loss of *Pten* resulted in changes in a broad range of water, ion, and organic transporters, which likely resulted in changes in the intracellular, intercellular microenvironment of epithelial cells, and epididymal lumen microenvironment, and eventually disrupting sperm maturation.

Materials and methods

Animals

Mice were handled according to the approved protocols following the guidelines of the Institutional Animal Care and Use Committee of the University of Virginia. Mice carrying *loxP*-flanked *Pten* allele (*Pten* $^{flox/flox}$) were purchased from The Jackson Laboratory (Bar Harbor, Maine). Tg(*Rnase10-Cre*) mice were a generous gift from Dr Huhtaniemi (Imperial College London, UK) [14]. Mice were bred and genotyped based upon the information provided by The Jackson Laboratory (Bar Harbor).

We defined epididymal regions according to previous studies [15, 16], which divided the epididymis into four major regions or 10 more defined regions: initial segment (I–II), caput (III–VI), corpus (VII–VIII), and cauda (IX–X).

RNAseq sequencing and analysis

Tissues from region I of the epididymis were dissected from 6-month-old control and knockout mice. Total RNA was extracted using Qiagen RNeasy Plus Mini Kit (Valencia, CA) according to the manufacturer's instructions. RNAsamples from the same animals were used to perform real-time PCR and RNAseq gene expression analysis. Quality control of RNA was conducted using TapeStation and qPCR methods at the Beckman Coulter Genomics (Danvers, MA). Complementary DNA synthesis and library construction were performed using Illumina Truseq RNASeq (San Diego, CA). Three control and three knockout sample replicates were analyzed on an Illumina HiSeq 2000 instrument at the Beckman Coulter Genomics (Danvers).

Initial quality assessment of sequencing reads was conducted using FASTQC (http://www.bioinformatics.babraham.ac.uk/projects/fastqc/). After aligning data with STAR [17], counted reads were mapped to GENCODE genes using the featureCounts software in the Subread package [18]. DESeq2 Bioconductor package [19] in the R statistical computing environment was used to normalize count data and fit a negative binomial model to assess for differential gene expression between knockout and control samples. The Benjamini–Hochberg false discovery rate (FDR) procedure was used to estimate adjusted *P*-values for GENCODE/Ensembl gene IDs mapping to known genes. The RNAseq data are available in GEO under accession (http://www.ncbi.nlm.nih.gov/geo/query/acc.cgi?acc = GSE92614). The following secure token has been created to allow review of record GSE92614 while it remains in private status: uhcbmygebtsfzyv.

To search over-represented or under-represented biological processes, cellular components, molecular functions, and signal pathways, the differentially expressed gene lists generated from RNAseq analysis were submitted to Gene Ontology (www.geneontology.org) and Ingenuity Pathway Analysis (www.ingenuity.com) for the enrichment and pathway analysis.

Data acquisition from public resource and microarray analysis

Dataset GSE24691 (http://www.ncbi.nlm.nih.gov/geo/query/acc.cgi?acc=GSE24691) was downloaded from the GEO website. Data samples (GSM608357, GSM608358, GSM608359, GSM608360) from prostate tissues of 3-month-old control mice (*Pten* floxed mice) and data samples (GSM608364, GSM608365, GSM608366, GSM608367) of prostate-specific *Pten* knockout mice were selected for microarray analysis. Statistically significant differences in mRNA abundance between control and knockout samples were determined using Linear Models for Microarray Data. The differentially expressed gene lists were used for further analysis.

Dataset GSE70681 (https://www.ncbi.nlm.nih.gov/geo/query/acc.cgi?acc=GSE70681) was selected from GEO website. Five control data samples (GSM1816399, GSM1816400, GSM1816401, GSM1816402, and GSM1816403) and three liver-specific *Pten* knockout samples (GSM1816404, GSM1816405, and GSM1816406) from 15-month-old mice were subjected to GEO2R analysis, a build-in tool in GEO website. Top 250 differentially expressed gene lists were used for further analysis.

Dataset GSE6078 (https://www.ncbi.nlm.nih.gov/geo/query/acc.cgi?acc=GSE6078) was selected from GEO website. Two data samples (GSM140792 and GSM140816) from control mouse intestines and three data samples (GSM140813, GSM140817, and GSM140818) from *Pten* knockout polyps were used for further analysis. This dataset in the GEO website has already been curated.

Immunofluorescence

Epididymal tissue samples were immersion-fixed in 4% paraformaldehyde (PFA) in phosphate buffered saline overnight at 4°C and followed by paraffin embedding and sectioning. Knockout and control sections were placed on the same slide side by side to ensure similar treatment. Subsequently, slides were deparaffinized and rehydrated. For antigen retrieval, slides were microwaved in antigen unmasking solution (Vector Laboratories, Burlingame, CA) for 10 min on high in a 1300 W microwave and cooled for 1 h at room temperature. Following blocking in blocking solution with 10% (v/v) normal goat or donkey serum (Vector Laboratories, 0.5% (v/v) gelatin from cold-water fish skin (Sigma, St. Louis, MO), and TBS for 1.5 h, slides were incubated overnight at 4°C in blocking solution with primary antibodies. Following washing in TBS, slides were incubated with 1:200 dilution of Alexa Fluor 594 secondary antibodies (Molecular Probe, Eugene, OR) in blocking solution for 1.5 h at room temperature. All slides were washed in TBS and mounted using Prolong Anti-fade reagent with DAPI (4,6-Diamidino-2-phenylindole) for nuclear staining (Molecular Probe, Eugene, OR) and were viewed under a Zeiss microscope equipped with epifluorescence. The following primary antibodies were purchased from Abcam (Cambridge, MA): NIPAL4 antibody (ab107979, 1:50 working dilution) and SLCO1C1 antibody (ab83972, 1:50 working dilution). Immunofluorescence labeling using goat anti-rabbit secondary antibody alone was performed to serve as negative controls for NIPAL4 and SLCO1C1 antibodies. Two antibodies were purchased from Santa Cruz Biotechnology (Santa Cruz, CA): ATP6V1B1 (V-ATPase B1) antibody (sc-21206, 1:50 working dilution) and ATP1A1 (Na^+K^+-ATPase $\alpha 1$) antibody (sc-21712, 1:50 working dilution). Immunofluorescence labeling using donkey anti-goat secondary antibody alone was performed to serve as a negative control for ATP6V1B1 antibody. Immunofluorescence labeling using mouse normal IgG as a primary antibody was performed to serve as a negative control for ATP1A1antibody. Supplementary Table S1 lists antibody information in detail.

Measurement of epithelial permeability

Fifty microliters of fluorescein isothiocyanate–dextran (FITC-dextran, 4000 Da; 5 mg/ml; Sigma-Aldrich) was injected into the mice tail vein. Thirty minutes following injection, epididymal tissues were harvested and immediately fixed in 4% PFA for 2 h. Tissues from the initial segment region I were hand-cut to small pieces and subjected to confocal imaging under a Zeiss 700 microscope.

Statistics

One-way analysis of variance was performed to identify significant changes. The significant difference was indicated by $*$ ($P < 0.05$) and $**$ ($P < 0.01$).

Results

Verification of RNAseq data with real-time PCR

In our previous publication, real-time PCR was employed to quantify mRNA levels of several genes [2] in epididymal region 1. In this study, mRNA levels of the entire transcriptome were measured using RNAseq sequencing. When comparing the mRNA levels of *Ros1*, androgen receptor (*Ar*), dual specificity phosphatase 6 (*Dusp6*,) and ets variant 4 (*Etv4*) measured by these two methods, the fold changes between knockouts and controls were similar (Supplementary Figure S1), confirming the accuracy of the RNAseq data.

Changes in the mRNA levels of water, ion, and organic solute transporters following loss of *Pten*

A broad range of water, ion, and organic solute transporters had significant changes in their mRNA levels following loss of *Pten*.

First, the top 500 differentially expressed genes based on FDR-adjusted *P*-value were subjected to Gene ontology enrichment analysis. Transporter activity was one of the top dysregulated molecular functions with *P*-value 7.83E-07 using Fisher's exact test. Fifty-three genes among the top 500 differentially expressed genes encoded transporter genes. Among these 53 genes, 38 transporter genes, including solute carriers, ATP-binding cassette (ABC) transporters, ATPase transporters, K^+, and other ion transporters showed more than twofold changes (Table 1), and 15 had more than fourfold changes in their mRNA levels following loss of *Pten*.

Second, 211 genes, which showed fourfold changes in their mRNA levels and had FDR-adjusted *P*-value less than 1%, were subjected to Ingenuity Pathway Analysis. Molecular transport was the top dysregulated molecular and cellular functions with *P*-value 1.61E-05 analyzed by Fisher's exact test. A total of 52 genes among the 211 differential expressed genes were involved in dysregulation of transport of molecules, concentration of lipids, absorption of K^+, and uptake of D-glucose (Figure 1).

Changes in ATPase transporters and ABC transporters following loss of *Pten*

Multiple ATPase transporters and ABC transporters showed differential expression in mRNA levels (FDR-adjusted *P*-value < 0.01) in knockouts compared to controls (Supplementary Tables S2 and S3).

ATP6V1B1 is a subunit of H^+ ATPase (also known as V-ATPase) and is a marker of narrow and clear cells [20]. According to RNAseq analysis, the *Atp6v1b1* mRNA level in knockouts was 3.0 times of the level in controls (Supplementary Table S2). ATP6V1B1 protein was localized to the plasma membrane and cytoplasmic of narrow cells. In controls, initial segment narrow cells elongated in the direction of apical–basal axis and always contacted the lumen with their apical surface protruded to the lumen (Figure 2A, yellow arrow). In knockouts, ATP6V1B1-positive narrow cells did not always have the elongated shape, and immunolocalization showed that a large percentage (44.3%, n = 127) of ATP6V1B1-positive narrow cells had lost their contact with the lumen (Figure 2B, yellow arrowheads).

ATP1 (Na^+-K^+ ATPase) regulates cellular Na^+ and K^+ levels and fluid volume [21]. Data from the RNAseq analysis showed mRNA levels of two genes that encode subunits of ATP1, *Atp1a1* and *Atp1b1*, increased to 1.3 and 2.0 times respectively following loss of *Pten* (Supplementary Table S2). ATP1A1 protein showed basolateral membrane localization in epithelial cells in controls (Figure 2C). In knockouts, ATP1A1 was also localized to the cell membrane of epithelial cells, but the intensity varied from one group of cells to another (Figure 2D).

The negative controls labeled with secondary anti-goat antibody alone or normal mouse IgG followed by secondary anti-mouse antibody are shown in Supplementary Figure S2A and B.

Table 1. Thirty eight transporters showing more than twofold change in their mRNA levels.

Category	Symbol	Gene name	Fold change	Up or down
Solute carriers	*Slco2a1*	Solute carrier organic anion transporter family, member 2a1	4.5	Up
	Slco1c1	Solute carrier organic anion transporter family, member 1c1	24.0	Up
	Slc46a2	Solute carrier family 46, member 2	11.0	Up
	Slc22a23	Solute carrier family 22, member 23,	4.2	Up
	Slc47a2	Solute carrier family 47, member 2	4.6	Down
	Slc2a5	Solute carrier family 2 (facilitated glucose transporter), member 5	4.5	Up
	Slc41a3	Solute carrier family 41, member 3	2.7	Down
	Slc7a11	Solute carrier family 7(cationic amino acid transporter y + system), member11	2.8	Down
	Slc29a4	Solute carrier family 29 (nucleoside transporters), member 4	3.4	Down
	Slc2a9	Solute carrier family 2 (facilitated glucose transporter), member 9	3.8	Up
	Slc7a4	Solute carrier family 7 (cationic amino acid transporter, y + system), member 4	2.1	Up
	Slc22a18	Solute carrier family 22 (organic cation transporter), member 18	2.8	Up
	Slc16a4	Solute carrier family 16 (monocarboxylic acid transporters), member 4	2.1	Down
	Slc6a13	Solute carrier family 6 (neurotransmitter transporter, gaba), member 13	3.5	Down
ABC transporters	*Abcb9*	ATP -binding cassette, sub-family b (mdr/tap), member 9	2.2	Down
	Abcc3	ATP-binding cassette, sub-family c (cftr/mrp), member 3	2.1	Up
ATPase transporters	*Atp4a*	ATPase, H^+-K^+ exchanging, gastric, alpha polypeptide	9.1	Up
	Atp11a	ATPase, class VI, type 11a	2.1	Up
Potassium channels	*Kcna1*	Potassium voltage-gated channel, shaker-related subfamily, member 1	6.5	Up
	Kcnc3	Potassium voltage gated channel, shaw-related subfamily, member 3	8.6	Up
	Kcnq1	Potassium voltage-gated channel, subfamily q, member 1	2.4	Up
Other ion channels	*Trpv6*	Transient receptor potential cation channel, subfamily v, member 6	2.5	Up
	Scnn1b	Sodium channel, nonvoltage-gated 1 beta	3.8	Up
Others	*Mfsd2a*	Major facilitator superfamily domain containing 2a	5.7	Down
	Nipal4	Nipa-like domain containing 4	5.8	Down
	Lcn5	Lipocalin 5	5.0	Up
	Steap2	Six transmembrane epithelial antigen of prostate 2	4.5	Down
	Syt2	Synaptotagmin ii	4.3	Down
	Sypl2	Synaptophysin-like 2	7.5	Up
	Ap1s2	Adaptor-related protein complex 1, sigma 2 subunit	2.4	Up
	Vldlr	Very low density lipoprotein receptor	2.5	Down
	Hpn	Hepsin	3.4	Up
	Cnga2	Cyclic nucleotide gated channel alpha 2	3.1	Up
	Trf	Transferrin	3.6	Down
	Anxa6	Annexin a6	2.2	Up
	Sec14l2	sec14-like 2	2.5	Up
	Cftr	Cystic fibrosis transmembrane conductance regulator	2.1	Down
	Rhbg	Rhesus blood group-associated b glycoprotein	2.3	Up

Changes in the protein levels of some transporters following loss of *Pten*

NIPAL4 (NIPA-like domain containing 4) is a membrane-associated protein, which acts as a Mg^{2+} transporter and can also transport other divalent cations but to a much less extent [22]. Data from RNAseq analysis showed *Nipal4* mRNA levels to have decreased 5.8 times following loss of *Pten* (Table 1). NIPAL4 proteins were localized to the apical membrane of epithelial cells (Figure 3A, yellow arrows) and had intensive labeling on the protruded apical membrane (Figure 3A, yellow arrowhead). The intensive labeling on the protruded apical membrane in control epithelial cells was absent in knockouts (Figure 3A and B).

The mRNA level of *Slco1c1* (solute carrier organic anion transporter family, member 1c) in knockout initial segments increased 24 times following loss of *Pten* (Table 1). SLCO1C1 proteins were localized to the apical area of some epithelial cells (Figure 3C and D, blue arrows), and the number of SLCO1C1-positive cells increased by 75 ± 8.1% in knockouts compared to controls (Figure 3C and D). The negative control labeled with secondary anti-rabbit antibody alone is shown in Supplementary Figure S2C.

Changes in permeability of the epithelium of the initial segment following loss of *Pten*

Following 30 min FITC-detran 4000 administration, a diffuse FITC signal was observed in control epididymal epithelial cells, while strong, punctate FITC-positive particles, which aggregated in the cytoplasm of epithelial cells in knockouts (Figure 4, arrow), were observed. Signal was undetectable in the lumen of control and knockout epididymides.

Changes in transporter activity following loss of *Pten* in other organs

Microarray gene expression data were acquired from the prostate tissues of 3-month-old prostate-specific *Pten* knockouts and controls (*Pten* floxed mice). Loss of *Pten* resulted in changes of a broad range of genes in the mRNA levels. When the top 500 differentially expressed genes were subjected to gene enrichment analysis in Gene ontology, a total of 46 genes among the 431 annotated genes were involved in transporter activity. Positive regulation of transport was one of the major dysregulated biological processes with *P*-value 8.20E-4 analyzed by Fisher's exact test.

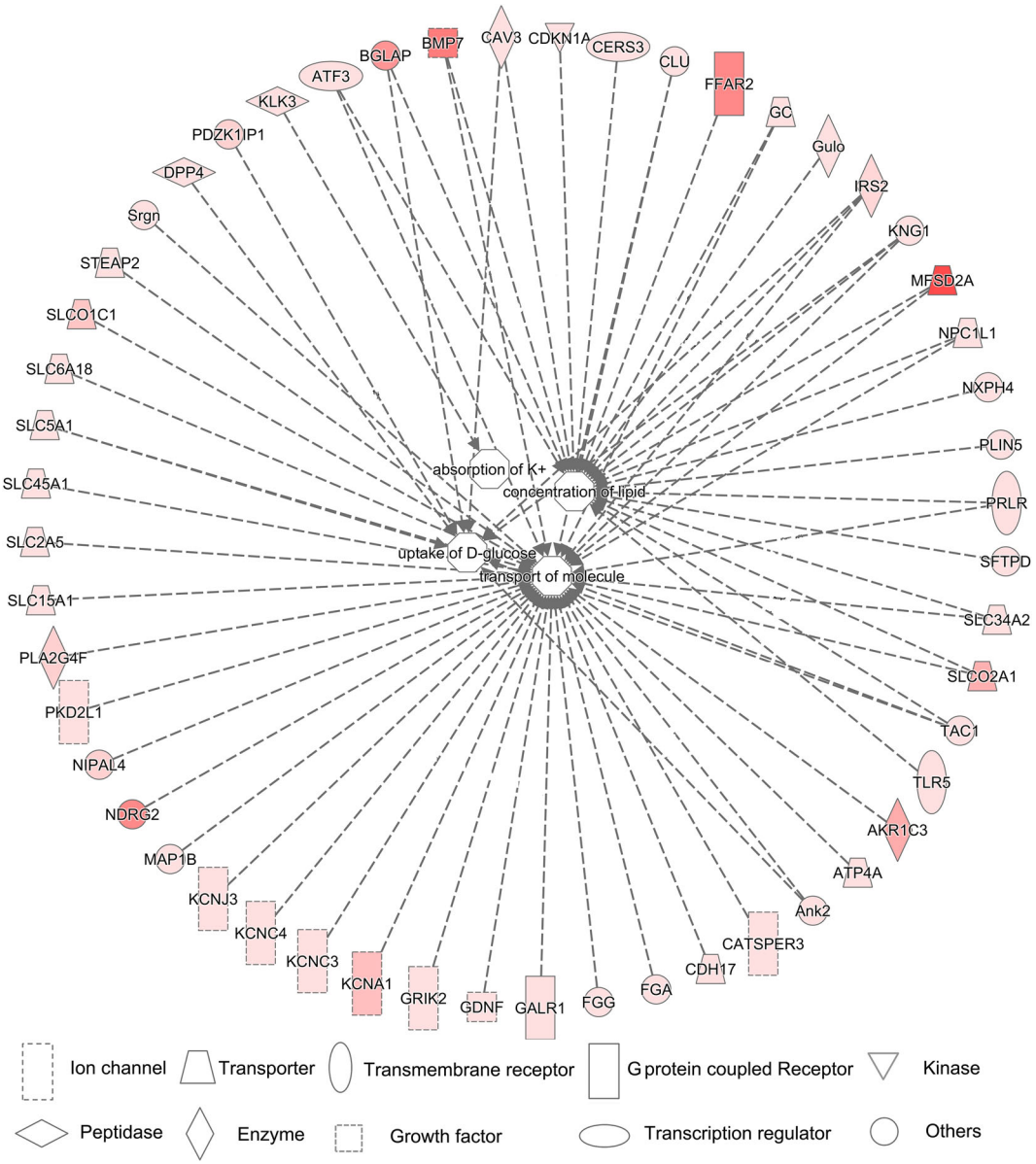

Figure 1. Fifty-two genes of the 211 top differentially expressed genes involved in the transport of molecules, concentration of lipid, uptake of D-glucose, and absorption of K^+. The greater the red color intensity indicates the greater the difference in expression of that gene between control and knockout tissues based on FDR adjusted *P-values*.

Loss of *Pten* in albumin expressing cells resulted in liver steatosis and spontaneous liver tumors. Microarray gene expression data were acquired from liver tissues of 15-month-old knockouts and controls. The top 250 differentially expressed genes were subjected to gene enrichment analysis in Gene ontology, and a total of 43 genes of the 228 annotated genes were involved in transporter activity. Regulation of transport was one of the major dysregulated biological processes with *P*-value 2.06E-3 analyzed by Fisher's exact test.

Deletion of *Pten* gene from the intestine resulted in intestinal polyps. Microarray gene expression data from *Pten* mutant intestinal polyps and control intestinal of 1-month-old mice were curated on the GEO website. A total of 374 genes were differentially expressed following loss of *Pten*. Transmembrane transport of small molecules was one of the major dysregulated pathways based on the GEO website.

Discussion

Our previous study established a male infertile mouse model by conditional deletion of *Pten* from the proximal epididymis [2]. In this study, we investigated transporter activity and epithelial permeability of this mouse model in the epididymis to better understand the mechanisms that regulate the epididymal luminal fluid microenvironment and sperm maturation.

Pten regulated a broad range of transporters in the epididymis

In the initial segment of the epididymis, a broad range of transporter genes showed changes in their mRNA levels and/or protein localization following loss of *Pten*. First, changes in many ion and water transporters including Na^+-K^+ ATPase subunits e.g. *Atp1a1*

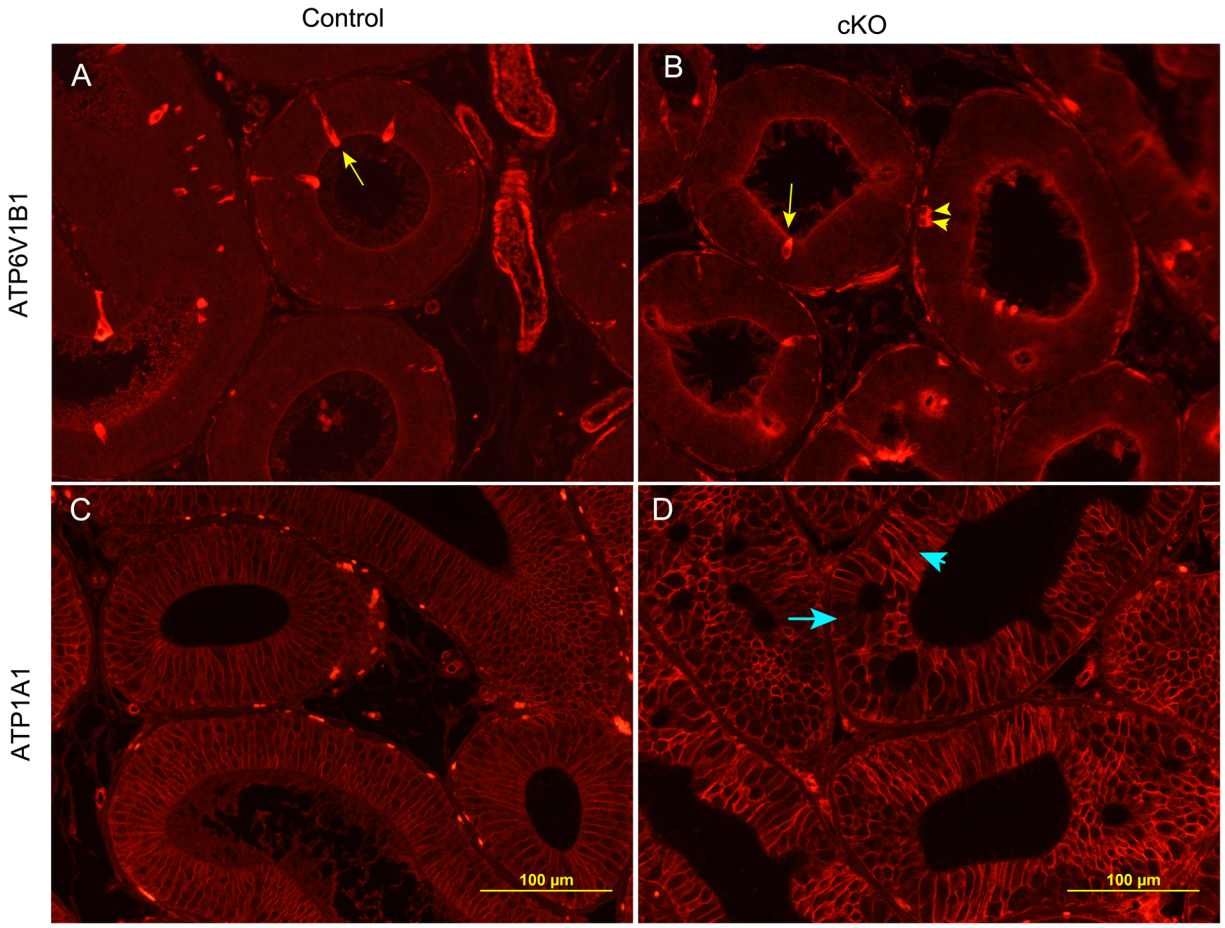

Figure 2. Immunolocalization of ATP6V1B1 and ATP1A1 in 6-month-old initial segments of controls and IS-specific *Pten* KOs. (A and B) Representative images of ATP6V1B1 localization in the narrow cells of controls and conditional knockouts (cKO). Yellow arrows show elongated narrow cells that are in contact with the lumen, and yellow arrowheads show round narrow cells without luminal contact. (C and D) Representative images of membrane localization of ATP1A1 in epithelial cells of the control and knockout initial segments. The blue arrow and blue arrowhead show two groups of cells with different labeling intensity.

and *Atp1b1*, H^+-K^+ exchangers e.g. *Atp4a*, Na^+-H^+ exchangers e.g. *Slc9a1* and *Slc9a2*, H^+ ATPase subunits e.g *Atp6v1b1*, K^+ channels e.g. *Kcna1*, *Kcnc3*, and *Kcnq1*, and aquaporins e.g. *Aqp9* were found in the initial segment following loss of *Pten*. This would suggest that *Pten* regulated ion and water transporters, and likely, there were changes in ion and water homeostasis in the epididymis of IS-specific *Pten* KO mice. Second, changes in many organic solute transporters, e.g. *Slcolc1* and *Slco2a*, and ABC transporters, e.g. *Abcc3* and *Abcb9*, were also detected in the initial segment following loss of *Pten*. These data would suggest that *Pten* also regulated organic solute transporters, which in turn may have resulted in a loss of protection from osmotic and/or chemical stress in the epididymis of IS-specific *Pten* KO mice.

Although there have been limited previous studies examining the functions of such a broad range of transporters in the epididymis, many individual transporters have been studied extensively to understand their function in the regulation of the epididymal luminal fluid microenvironment [20, 21, 23–26].

First, several water and ion transporters including Na^+-K^+ATPase, Na^+-H^+exchangers, H^+ATPase (V-ATPase), and aquaporins (AQPs) have been found to be essential for epididymal function [20, 21, 23, 24]. For example, clear cells, which are also known as narrow cells in the initial segment, have a high level of expression of the proton pump V-ATPase in the plasma membrane of epididymal epithelial cells. V-ATPase is involved in acidification of luminal fluid, a process that is important for sperm maturation; loss of V-ATPase subunits causes male infertility [20, 24].

Second, many organic solute transporters have also been studied in the epididymis, including ABC family of efflux transporters, amino acid transporters, and glucose transporters [21]. Among the organic solute transporters, ABC transporters including ABCB1 (phosphoglycoprotein and multidrug resistance-1) and ABCG2 (breast cancer resistance protein and mitoxantrone resistance protein) were responsible for efflux of many xenobiotics and toxicants from tissues and were expressed in the epididymis [25]. The administration of phytoestrogens to *Abcg2* knockout mice resulted in elevated epididymal concentrations of phytoestrogens as compared with wild-type mice, suggesting its role in protecting the epididymis from chemical insult [26]. In addition, several antifertility agents affected male fertility through interfering with sugar transport in the epididymis, suggesting that sugar transport played a role during sperm maturation [27, 28].

Since changes in certain individual transporters affected the luminal fluid microenvironment and sperm maturation process [20–28], it is not surprising that changes in a broad range of transporters

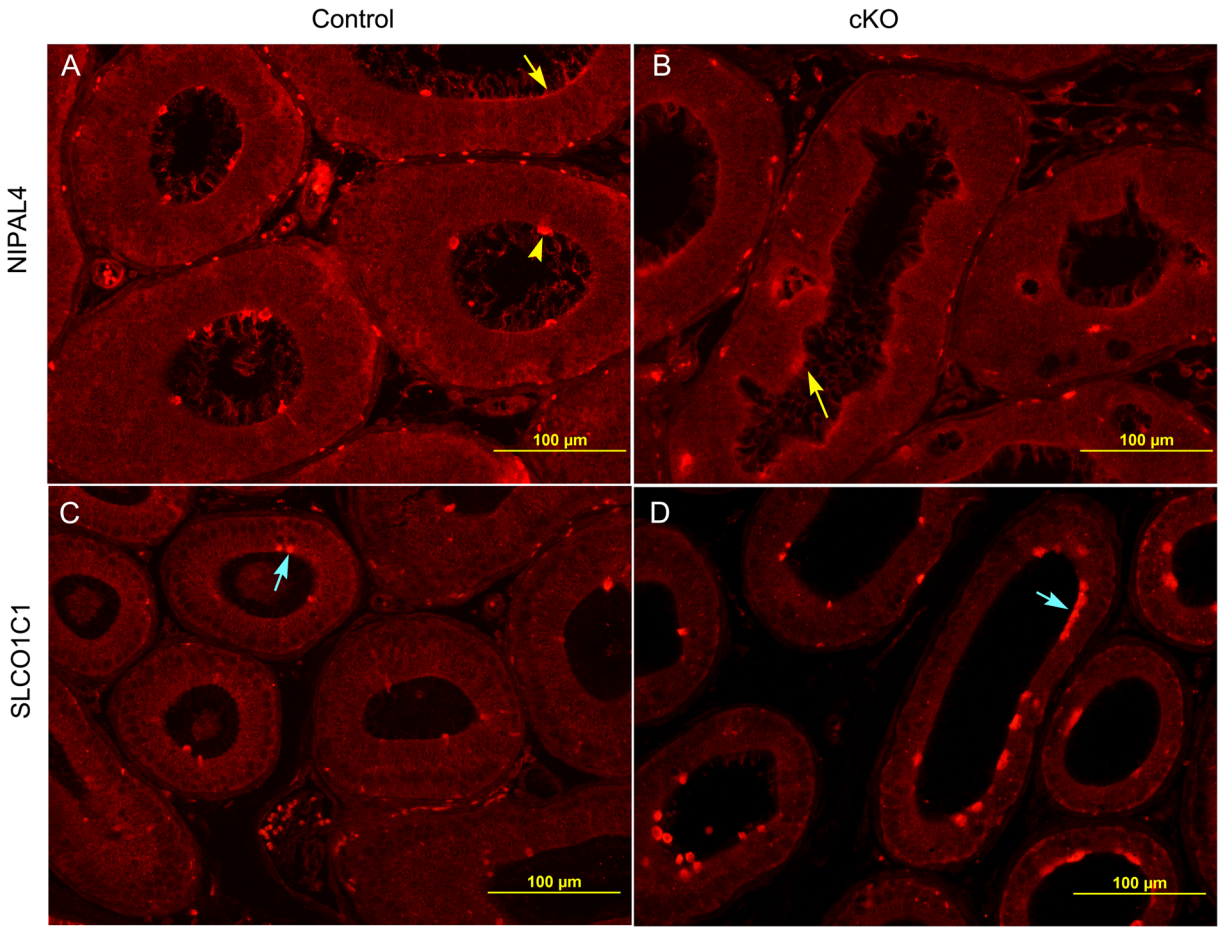

Figure 3. Immunolocalization of NIPAL4 and SLCO1C1 in 6-month-old initial segments of controls and IS-specific *Pten* KOs. (A and B) Representative images of apical localization of NIPAL4 in the initial segment of controls and conditional knockouts (cKO). Yellow arrows show apical location of NIPAL4 in the epithelium, and yellow arrowhead shows intensive NIPAL4 labeling at apical protrusions. (C and D) Representative images of apical localization of SLCO1C1 in control and knockout initial segments. Blue arrows label punctate apical localization of NIPAL4 in the epithelium.

in IS-specific *Pten* KOs compared to controls would disrupt sperm maturation function.

When FITC-detran 4000 was administrated systemically, it did not pass through the epididymal tight junctions, suggesting that tight junctions were intact in the epididymis of IS-specific *Pten* KOs. This is consistent with our previous report, which had shown normal localization of several tight junction protein markers [2]. An increase in the accumulation of FITC-detran 4000 in the epididymal epithelium of IS-specific *Pten* KOs compared to controls suggested changes in the transepithelial transport of molecules, for example, endocytosis and/or pinocytosis.

Pten regulated transporter activity in other organs

Previous studies revealed a common finding that PTEN regulated cell shape, size, and organization, likely through regulation of the PI3K/AKT pathway [2, 29]. Increased cell size has accounted for hypertrophy phenotypes observed in multiple tissue-specific *Pten* knockout models including our IS-specific *Pten* KOs [2, 29]. More importantly, alteration in cell size, shape, and organization would change the properties of the basolateral and apical membranes. Therefore, it is reasonable to hypothesize that changes in these membrane properties would likely change a broad range of transporter activities in many cell types following loss of *Pten*. To test this hypothesis, we analyzed the microarray data from prostate, intestine, and liver-specific *Pten* knockouts. Regulation of ion, water, and organic solute transporters was indeed one of enhanced biological processes following loss of *Pten*, suggesting a common role of PTEN in the regulation of transport of molecules.

Unlike the tumor suppression function of PTEN, the transporter regulation function of PTEN has not been systematically studied. However, evidence from previous studies has showed that PTEN regulates the activities of different transporters in multiple organs and cell types [29–34]. Specific deletion of *Pten* in the lens frequently led to the development of a cataract. The study of *Pten* insufficiency-associated cataract identified a direct role for *Pten* in the regulation of lens Na^+-K^+ATPase activity through an AKT-dependent modulation [30]. In thyroid cancer cells, loss of *Pten* was associated with increased expression of SLC2A1 on the plasma membrane. SLC2A1 was also known as glucose transporter 1, and increased SLC2A1 expression was associated with an increase in glucose uptake [31]. It was also concluded that PTEN functioned as a suppressor of glucose transport through the PI3K pathway in adipocytes [32]. In chronic myeloid leukemia, *Pten* regulated ABCG2 transporter [33]. More recently, PTEN was shown to be involved in regulation of glutamate aspartate transporter in the adult optic nerve [34].

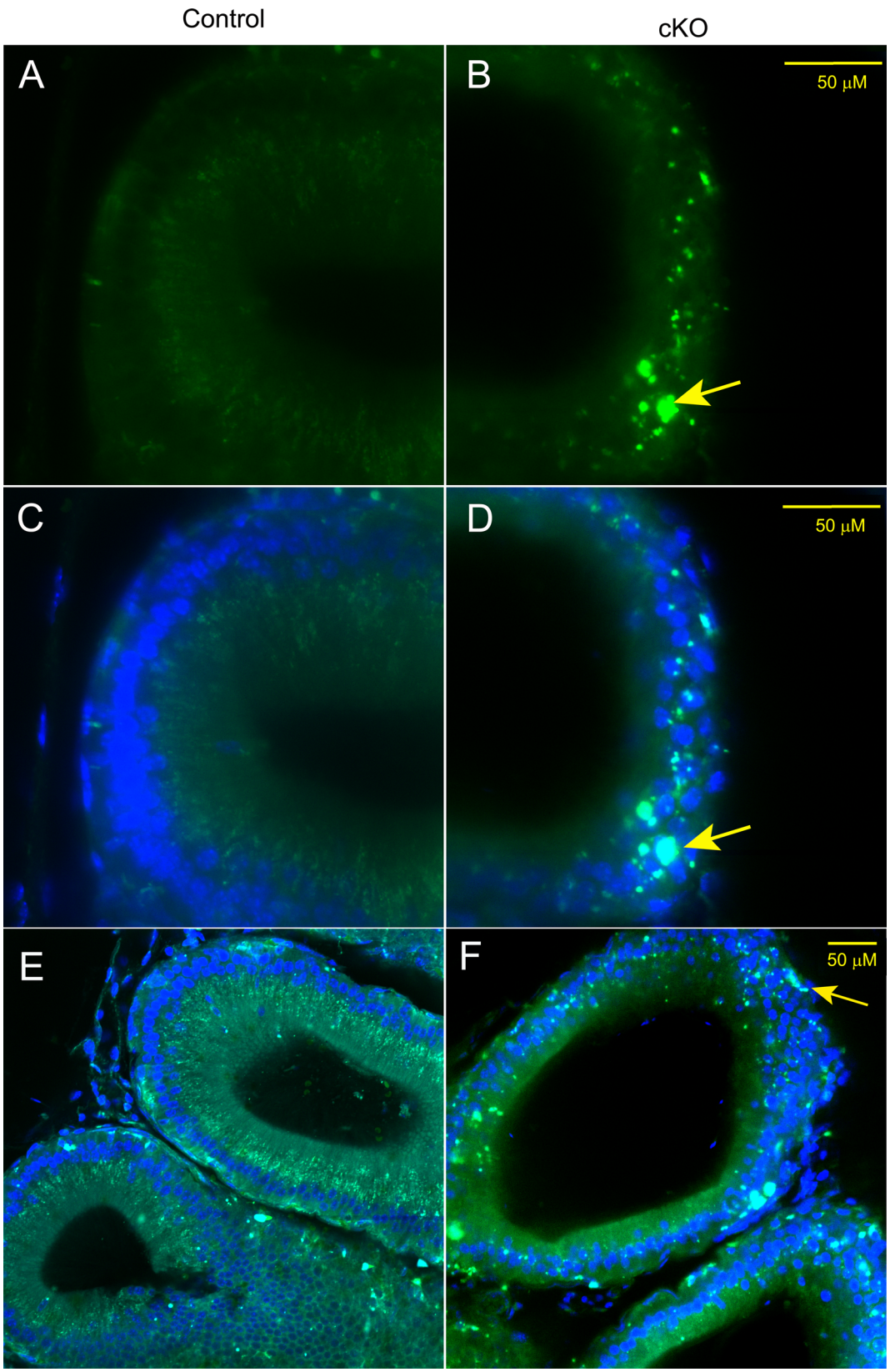

Figure 4. Permeability of FITC-detran 4000 in epithelial cells of control and knockout initial segments. (A and B) High magnification images. (C and D) High magnification images merged with DAPI nuclear staining. (E and F) Low magnification images merged with DAPI nuclear staining. Note a diffuse FITC signal in epididymal epithelial cells in controls and strong punctate FITC-positive particles aggregated in the cytoplasm of epithelial cells in knockouts (yellow arrow).

In summary, our data coupled with previous reports suggested that PTEN regulated a broad range of transporters in many organs and cell types. In the epididymis, changes in transporter activity following loss of *Pten* would presumably result in an alteration of the luminal fluid microenvironment resulting in male infertility. Future studies will focus on the examination of the composition of the initial segment luminal fluid in *Pten* knockout mice to test the hypothesis that changes in the luminal fluid microenvironment were the result of changes in transporter activity.

Supplementary data

Supplementary data are available at *BIOLRE* online.

Supplementary Figure S1. Comparison of real-time PCR and RNAseq analysis on the changes of mRNA levels of *Ros1, Ar, Dusp6,* and *Etv4* following loss of *Pten*. Samples from the same animals were examined using real-time PCR and RNAseq. The average mRNA levels in controls were set as 1, and the relative values in conditional knockouts (cKO) were then calculated. Data are represented as mean ± SEM.

Supplementary Figure S2. Control images of initial segments showing the level of background immunofluorescence. (A) Degree of fluorescence when donkey anti-goat secondary antibody was used alone. (B) Degree of fluorescence when a primary antibody was replaced by normal mouse IgG. (C) Degree of fluorescence when goat anti-rabbit secondary antibody was used alone. Longer exposure times were purposely used in these images to demonstrate the low degree of background fluorescence.

Supplementary Table S1. Antibody information.

Supplementary Table S2. Differentially expressed ATPase transporters following loss of *Pten*.

Supplementary Table S3. Differentially expressed ABC transporters following loss of *Pten*.

Acknowledgment

We thank Angela M. Washington for her assistance in performing experiments.

References

1. Knobbe CB, Lapin V, Suzuki A, Mak TW. The roles of PTEN in development, physiology and tumorigenesis in mouse models: a tissue-by-tissue survey. *Oncogene* 2008; **27**:5398–5415.
2. Xu B, Washington AM, Hinton BT. PTEN signaling through RAF1 proto-oncogene serine/threonine kinase (RAF1)/ERK in the epididymis is essential for male fertility. *Proc Natl Acad Sci USA* 2014; **111**:18643–18648.
3. Sonnenberg-Riethmacher E, Walter B, Riethmacher D, Godecke S, Birchmeier C. The c-ros tyrosine kinase receptor controls regionalization and differentiation of epithelial cells in the epididymis. *Genes Dev* 1996; **10**:1184–1193.
4. Sipila P, Cooper TG, Yeung CH, Mustonen M, Penttinen J, Drevet J, Huhtaniemi I, Poutanen M. Epididymal dysfunction initiated by the expression of simian virus 40 T-antigen leads to angulated sperm flagella and infertility in transgenic mice. *Mol Endocrinol* 2002; **16**:2603–2617.
5. Cooper TG, Yeung CH. Acquisition of volume regulatory response of sperm upon maturation in the epididymis and the role of the cytoplasmic droplet. *Microsc Res Tech* 2003; **61**:28–38.
6. Cooper TG, Yeung CH, Wagenfeld A, Nieschlag E, Poutanen M, Huhtaniemi I, Sipila P. Mouse models of infertility due to swollen spermatozoa. *Mol Cell Endocrinol* 2004; **216**:55–63.
7. Yeung CH, Anapolski M, Setiawan I, Lang F, Cooper TG. Effects of putative epididymal osmolytes on sperm volume regulation of fertile and infertile c- ros transgenic mice. *J Androl* 2004; **25**:216–223.
8. Yeung CH, Anapolski M, Sipila P, Wagenfeld A, Poutanen M, Huhtaniemi I, Nieschlag E, Cooper TG. Sperm volume regulation: maturational changes in fertile and infertile transgenic mice and association with kinematics and tail angulation. *Biol Reprod* 2002; **67**:269–275.
9. Yeung CH, Sonnenberg-Riethmacher E, Cooper TG. Infertile spermatozoa of c-ros tyrosine kinase receptor knockout mice show flagellar angulation and maturational defects in cell volume regulatory mechanisms. *Biol Reprod* 1999; **61**:1062–1069.
10. Turner T. Necessity's potion: inorganic ions and small organic molecules in the epididymal lumen. In: Robaire B HB (ed.) *The Epididymis: From Molecules to Clinical Practice*, 4th ed. New York: Kluwer Academic/Plenum Publishers; 2002: 131–150.
11. Cooper TG. Sperm maturation in the epididymis: a new look at an old problem. *Asian J Androl* 2007; **9**:533–539.
12. Wagenfeld A, Yeung CH, Lehnert W, Nieschlag E, Cooper TG. Lack of glutamate transporter EAAC1 in the epididymis of infertile c-ros receptor tyrosine-kinase deficient mice. *J Androl* 2002; **23**:772–782.
13. Yeung CH, Breton S, Setiawan I, Xu Y, Lang F, Cooper TG. Increased luminal pH in the epididymis of infertile c-ros knockout mice and the expression of sodium-hydrogen exchangers and vacuolar proton pump H+-ATPase. *Mol Reprod Dev* 2004; **68**:159–168.
14. Krutskikh A, Poliandri A, Cabrera-Sharp V, Dacheux JL, Poutanen M, Huhtaniemi I. Epididymal protein Rnase10 is required for post-testicular sperm maturation and male fertility. *FASEB J* 2012; **26**:4198–4209.
15. Robaire B, Hermo L. Efferent duct, epididymis, and vas deferens: structure, functions, and their regulation. In: Knobil E, Neill J (eds.), *The Physiology Of Reproduction*, vol. **1**. New York: Raven Press; 1988: 999–1080.
16. Jelinsky SA, Turner TT, Bang HJ, Finger JN, Solarz MK, Wilson E, Brown EL, Kopf GS, Johnston DS. The rat epididymal transcriptome: comparison of segmental gene expression in the rat and mouse epididymides. *Biol Reprod* 2007; **76**:561–570.
17. Dobin A, Davis CA, Schlesinger F, Drenkow J, Zaleski C, Jha S, Batut P, Chaisson M, Gingeras TR. STAR: ultrafast universal RNA-seq aligner. *Bioinformatics* 2013; **29**:15–21.
18. Liao Y, Smyth GK, Shi W. featureCounts: an efficient general purpose program for assigning sequence reads to genomic features. *Bioinformatics* 2014; **30**:923–930.
19. Love MI, Huber W, Anders S. Moderated estimation of fold change and dispersion for RNA-seq data with DESeq2. *Genome Biol* 2014; **15**:550.
20. Breton S, Brown D. Regulation of luminal acidification by the V-ATPase. *Physiology (Bethesda)* 2013; **28**:318–329.
21. Robaire B, Hinton B. The epididymis. In: Plant T, Zeleznik AJ (eds.) *Knobil and Neill's Physiology of Reproduction*, 4th edn. New York: Elsevier; 2015: 691–772.
22. Lefèvre C, Bouadjar B, Karaduman A, Jobard F, Saker S, Ozguc M, Lathrop M, Prud'homme JF, Fischer J. Mutations in ichthyin a new gene on chromosome 5q33 in a new form of autosomal recessive congenital ichthyosis. *Hum Mol Genet*. 2004; **13**:2473–2482.
23. Kujala M, Hihnala S, Tienari J, Kaunisto K, Hastbacka J, Holmberg C, Kere J, Hoglund P. Expression of ion transport-associated proteins in human efferent and epididymal ducts. *Reproduction* 2007; **133**:775–784.
24. Pietrement C, Sun-Wada GH, Silva ND, McKee M, Marshansky V, Brown D, Futai M, Breton S. Distinct expression patterns of different subunit isoforms of the v-atpase in the rat epididymis. *Biol Reprod* 2006; **74**:185–194.
25. Jones SR, Cyr DG. Regulation and characterization of the ATP-binding cassette transporter-B1 in the epididymis and epididymal spermatozoa of the rat. *Toxicol Sci* 2011; **119**:369–379.
26. Enokizono J, Kusuhara H, Sugiyama Y. Effect of breast cancer resistance protein (Bcrp/Abcg2) on the disposition of phytoestrogens. *Mol Pharmacol* 2007; **72**:967–975.
27. Hinton BT, Hernandez H, Howards SS. The male antifertility agents alpha chlorohydrin, 5-thio-D-glucose, and 6-chloro-6-deoxy-D-glucose interfere

with sugar transport across the epithelium of the rat caput epididymidis. *J Androl* 1983; **4**:216–221.
28. Turner TT, D'Addario DA, Howards SS. The transepithelial movement of 3H-3-O-methyl-d-glucose in the hamster seminiferous and cauda epididymidal tubules. *Fertil Steril* 1983; **40**:530–535.
29. Backman S, Stambolic V, Mak T. PTEN function in mammalian cell size regulation. *Curr Opin Neurobiol* 2002; **12**:516–522.
30. Sellitto C, Li L, Gao J, Robinson ML, Lin RZ, Mathias RT, White TW. AKT activation promotes PTEN hamartoma tumor syndrome–associated cataract development. *J Clin Invest* 2013; **123**: 5401–5409.
31. Morani F, Phadngam S, Follo C, Titone R, Aimaretti G, Galetto A, Alabiso O, Isidoro C. PTEN regulates plasma membrane expression of glucose transporter 1 and glucose uptake in thyroid cancer cells. *J Mol Endocrinol* 2014; **53**:247–258.
32. Tang X, Powelka AM, Soriano NA, Czech MP, Guilherme A. PTEN, but not SHIP2, suppresses insulin signaling through the phosphatidylinositol 3-kinase/Akt pathway in 3T3-L1 adipocytes. *J Biol Chem* 2005; **280**:22523–22529.
33. Huang FF, Zhang L, Wu DS, Yuan XY, Yu YH, Zhao XL, Chen FP, Zeng H. PTEN regulates BCRP/ABCG2 and the side population through the PI3K/Akt pathway in chronic myeloid leukemia. *PLoS One* 2014; **9**:e88298.
34. Huang Z, Hu Z, Xie P, Liu Q. Tyrosine-mutated AAV2-mediated shRNA silencing of PTEN promotes axon regeneration of adult optic nerve. *PLoS One* 2017; **12**:e0174096.